





## Research Article

# Effect of Molybdenum Disulphide Thin Films on Enhancing the Performance of Polycrystalline Silicon Solar Cells

Rajasekar Rathanasamy <sup>1</sup>, Gobinath Velu Kaliyannan <sup>2</sup>, Santhosh Sivaraj <sup>3</sup>,  
Essakkiappan Muthiah <sup>1</sup>, Abdul Azeem Ajmal Khaan <sup>1</sup>,  
Dharmaprakash Ravichandran <sup>1</sup> and Md. Elias Uddin <sup>4</sup>

<sup>1</sup>Department of Mechanical Engineering, Kongu Engineering College, Perundurai, Tamil Nadu 638060, India

<sup>2</sup>Department of Mechatronics Engineering, Kongu Engineering College, Perundurai, Tamil Nadu 638060, India

<sup>3</sup>Department of Robotics and Automation, Easwari Engineering College, Ramapuram, Chennai, Tamil Nadu 600089, India

<sup>4</sup>Department of Leather Engineering, Faculty of Mechanical Engineering, Khulna University of Engineering and Technology, Khulna, Bangladesh

Correspondence should be addressed to Md. Elias Uddin; [eliasuddin@le.kuet.ac.bd](mailto:eliasuddin@le.kuet.ac.bd)

Received 30 May 2022; Revised 20 January 2023; Accepted 3 February 2023; Published 1 March 2023

Academic Editor: Daniel T. Cotfas

Copyright © 2023 Rajasekar Rathanasamy et al. This is an open access article distributed under the Creative Commons Attribution License, which permits unrestricted use, distribution, and reproduction in any medium, provided the original work is properly cited.

This research work focuses on augmenting the power conversion efficiency of the polycrystalline silicon solar cell with the aid of antireflection coating (ARC) of synthesized molybdenum disulphide ( $\text{MoS}_2$ ). The sol-gel technique and electrospraying method were preferred for synthesizing and depositing  $\text{MoS}_2$  as transparent thin films on the surface of the solar cells. The optical, electrical, structural, and thermal properties of the coated solar cells were analyzed for understanding the influence of the  $\text{MoS}_2$  coating. Five different samples (A-II, A-III, A-IV, A-V, and A-VI) were coated with varying coating time. Among them, 120 min coated sample experienced a maximum power conversion efficiency (PCE) of 17.96% and 18.82% under direct sunlight and neodymium light with resistivity as low as  $2.79 \times 10^{-3} \Omega\text{-cm}$ . The investigation of optical properties of the coated solar cells revealed a maximum transmittance of 93.6% and minimum reflectance of 6.3%, achieved for A-IV sample in the visible UV spectrum. Sample A-IV showed prominent results in the temperature analysis with temperatures as low as 38.9°C in uncontrolled and 43.2°C in controlled source environments. The results from various analyses proved that  $\text{MoS}_2$  was an appropriate material for an antireflection coating to enhance the performance of polycrystalline solar cell.

## 1. Introduction

The rapid consumption of fossil fuels has increased the demand for renewable energy [1]. Solar energy, one of the major contributors to the renewable energy industry, can be harnessed through photovoltaic cells (PV cells) [2]. The average power conversion efficiency (PCE) of these cells was usually around 12-15% due to various losses. Inorganic PV cells were highly stable in nature, hence delivering consistent power for longer period of time [3]. Moreover, organic PVs have also grasped the attention due to their low cost, tunable spectral response, and flexible nature. It can be installed over any curvature owing to considerable

magnitude of power conversion efficiency [4, 5]. The major loss which occurs in these solar cells was the reflective loss, also including charge recombination and energy loss [6]. 20-30% of the incident light was reflected from the surface of polycrystalline silicon solar cell which leads to a decrease in rated power conversion efficiency (PSSC) [7]. This drawback can be rectified through antireflective surface coatings and thereby increase the PCE of the solar cell [8, 9]. Antireflection coating (ARC) increases the transmittance of the solar cell by increasing its light trapping capacity resulting in enhanced solar cell performance [10]. The metal oxide semiconductors like  $\text{Al}_2\text{O}_3$  [11],  $\text{SiO}_2$  [12, 13],  $\text{ZnO}$  [14, 15], and  $\text{TiO}_2$  [16] have been extensively employed as ARC

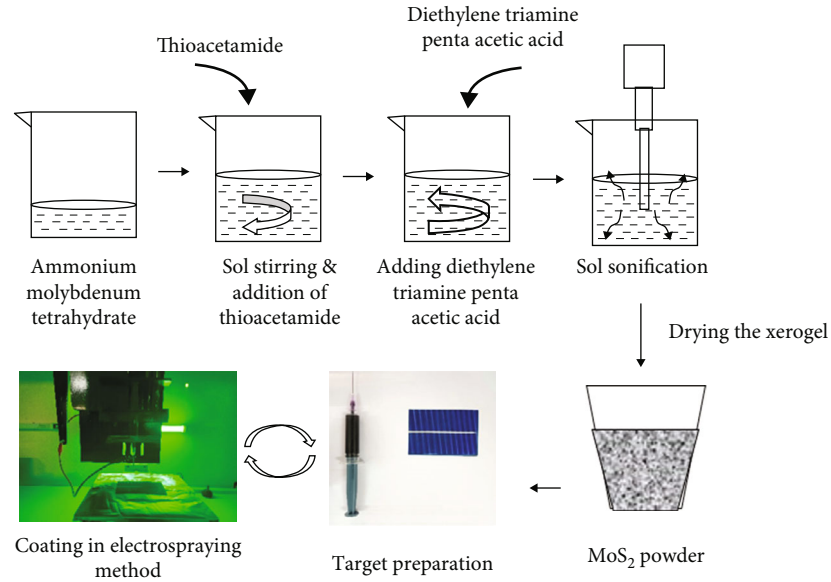


FIGURE 1: Pictorial representation of synthesis and deposition of MoS<sub>2</sub>.

TABLE 1: Deposition parameters for electro-spraying.

Deposition layers	Coating duration (min)	Flow rate (ml/hr)	Voltage (kV)	Substrate target distance (cm)
A-II	60			
A-IV	90			
A-IV	120	2	17	3
A-V	150			
A-VI	135			

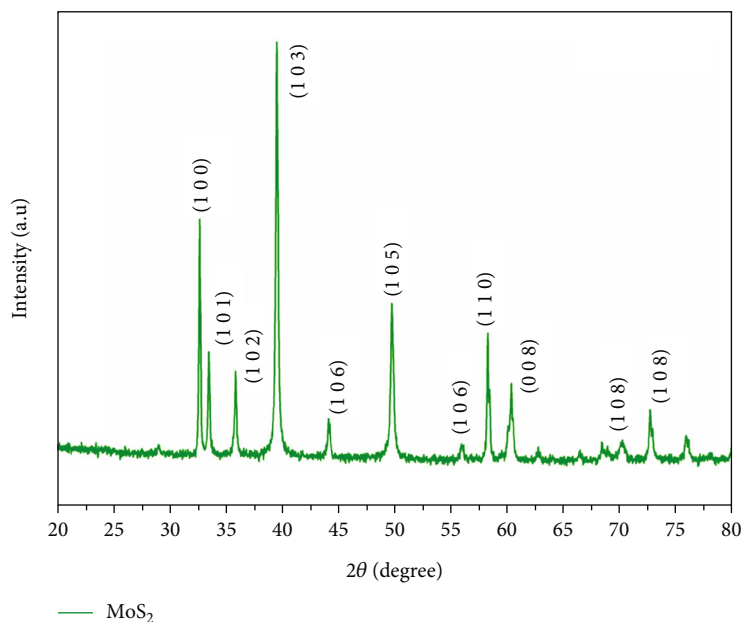
materials. In general, the transition metal dichalcogenides exhibit better optical and electrical properties [17]. Among the transition metal dichalcogenides, molybdenum disulphide (MoS<sub>2</sub>) has gained greater attraction in recent times. It was extensively utilized in photodetectors and supercapacitor electrode applications [18, 19].

The reduction in reflective losses depends on the quality of the coating which is influenced by parameters such as number of layers, coating thickness, and coating methodology [20, 21]. The methods employed for depositing the ARC materials as nano-thin films include thermal evaporation [22], spray pyrolysis [23], RF sputtering [10, 24, 25], plasma-enhanced chemical vapor deposition (PECVD) [26], atomic layer deposition [27], and electrospinning [28]. Sol-gel technique is a low-cost room temperature synthesis of nanomaterials after undergoing series of process such as aggregation, gelation, drying, and tempering [29].

This method provides an advantage of uniform deposition of droplets with sizes varying from micrometers to nanometers. Through electro-spraying technique, the dispersed solution was ejected at higher velocity forms a thin film. The thin film was dried only under the influence of higher input voltage (not due to the effect of temperature). The basic characteristics of thin film formed from electro-

spraying technique can be altered easily by changing the input operating conditions such as mass flow rate, substrate to target distance, type of collector, supply voltage, and viscosity of material. The heterostructured MoS<sub>2</sub> was employed as effective photodetector for X-ray imaging applications [30]. Transition metal chalcogenide MoS<sub>2</sub> with polycrystalline Si was used as heterojunction solar cells which have the tendency to absorb the incoming photons in minimal quantity and deliver equivalent photocurrent. Electro-spraying is one of the methods in which the deposition material solution is dispersed towards the target material charged with high electric potential [13]. This method provides an advantage of uniform deposition of droplets with sizes varying from micrometers to nanometers. The electro-spraying method enables us to control the coating parameters like time and flow rate of the deposition material [31, 32]. The MoS<sub>2</sub> was synthesized using the sol-gel method which enables us to produce high-quality thin films with low complexity [33]. Synthesized MoS<sub>2</sub> holds energy band gap of 1.35 eV and hence finds out the applications in detection of light and gas, energy storage systems [34], energy harvester, perovskite solar cells [35], optoelectronics, etc. [36]. The lab-scale thin film coating shows better uniformity than large-scale coating due to lesser working area. Almost uniform coating can be achieved in large-scale coating through proper optimization of operating parameters [37]. In this work, neodymium light was used in place of sunlight for analyzing the AR-coated Si solar cells. The color temperature of neodymium was 2800 K and emits light bluer in nature much similar to the sunlight. With the solar power meter and AC regulator, the intensity of neodymium light was matched with the solar radiation. The artificial solar light (neodymium) was used for evaluating the coated solar cell performance which possesses very minimal deviation in incident radiation.

This work is aimed at utilizing sol-gel-derived MoS<sub>2</sub> as the ARC material to increase the efficiency of PSSC through

FIGURE 2: X-ray diffraction pattern of synthesized MoS<sub>2</sub>.

electrospraying technique. The PCE of the samples was analyzed under controlled source environment using a neodymium lamp as the source of illumination and uncontrolled source environment (under direct sunlight). The obtained I-V values were used to interpret the influence of the coated films at varying operating conditions. Moreover, the structural, thermal, optical, and electrical properties of various MoS<sub>2</sub>-coated samples were evaluated to determine the performance of the polycrystalline silicon solar cells.

## 2. Experimental Techniques

The solar cells used in this research are polycrystalline solar Si solar cells bought from Vikram Solar, India.

**2.1. Methodology.** The work flow of the process which is depicted in Figure 1 includes the synthesis of MoS<sub>2</sub> and deposition of synthesized MoS<sub>2</sub> on solar cells, analyzing the electrical properties of the samples to understand the effects and inspecting the structural properties.

**2.2. Synthesis of MoS<sub>2</sub>.** Materials involved in the synthesis of MoS<sub>2</sub> were ammonium molybdate tetrahydrate, thioacetamide and diethylenetriaminepentaacetic acid which act as the sources of molybdenum and sulphur and chelating agent. The synthesis of MoS<sub>2</sub> dichalcogenide involves dissolving  $2 \times 10^{-4}$  kg ( $16 \times 10^{-3}$  mol) of (NH<sub>4</sub>)<sub>6</sub>Mo<sub>7</sub>O<sub>24</sub>·4H<sub>2</sub>O (ammonium molybdate tetrahydrate) in  $8 \times 10^{-3}$  litres of deionized water. The obtained solution was stirred constantly, and then 400 mg ( $5.3 \times 10^{-3}$  mol) of CH<sub>3</sub>CSNH<sub>2</sub> (thioacetamide) was added to the solution. With the obtained final solution, 0.05 grams of diethylenetriaminepentaacetic acid was added and stirred for 2 hours to attain the brown sol [30]. Then, sol was kept at 60°C in an oven for 13 hours which results in bronze gel formation. This xerogel

TABLE 2: Microstrain ( $\epsilon$ ), average crystallite size ( $t$ ), and dislocation density ( $\delta$ ) of synthesized MoS<sub>2</sub> particles.

2 $\theta$	$\beta$	$t$ (nm)	$\delta$ ( $\times 10^{-3}$ nm <sup>-2</sup> )	$\epsilon$ ( $\times 10^{-3}$ )
32.64037	0.78923	10.08963	9.823124989	11.76103531
32.68418	0.68023	11.70508	7.29879833	10.12237542
32.68418	0.68717	11.58686	7.44848904	10.22564826
39.54982	1.27147	6.140974	26.51706475	15.43090139
44.22005	1.00711	7.632933	17.16394428	10.81654037
49.8021	0.80639	9.332971	11.48048336	7.579682129
58.34622	0.94854	7.637902	17.14162089	7.413654527
60.41802	0.80641	8.891941	12.64756322	6.043420997
72.8043	1.97087	3.388512	87.09276291	11.66321959
76.02522	0.74654	6.647304	22.63126916	5.489879609

was dried for 2 days and further placed within a tubular furnace under argon gas atmosphere flowing at 180 sccm to form the powdered MoS<sub>2</sub> [38, 39].

**2.3. Electro Spray Deposition.** The calculated volume of synthesized MoS<sub>2</sub> was dissolved in ethanol and then stirred for 2 hours at room temperature to form appropriate coating solution. Ethanol was further used to clean the surface of the solar cells before coating. Then, the cells were placed in electrospinning setup, and the prepared solution was deposited as charged droplets through strong electrostatic force of attraction for varying time period. The electrospaying method enables the deposition material to be charged and dispersed as small droplets scaling from micrometers to nanometers.

The sample A-I indicates the bare uncoated cell. The samples A-II to A-VI indicate that MoS<sub>2</sub>-coated solar cells varied by coating time. During the analysis, a significant decline in the efficiency for sample A-V was found. It was

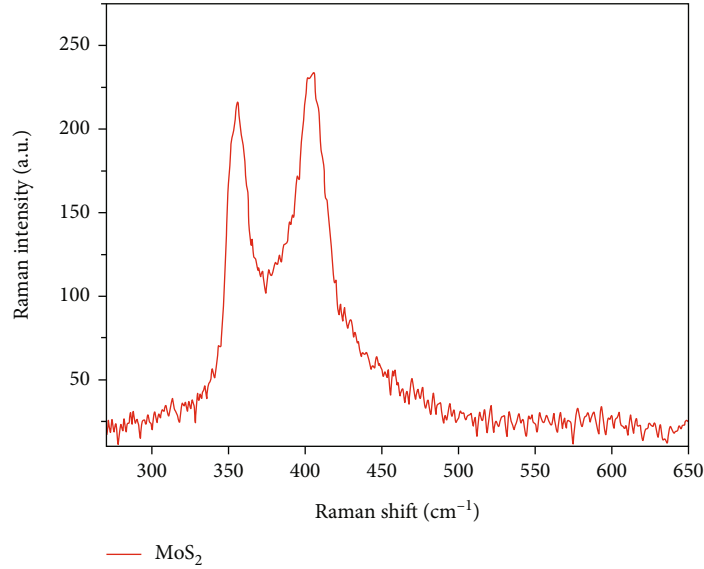


FIGURE 3: Raman spectra of the synthesized MoS<sub>2</sub>.

speculated that this was due to the excessive coating time period. To confirm the optimal coating time as 120 min and the decline of electrical properties in samples coated for greater than 120 min, another sample was coated with a coating time slightly longer than A-IV (135 min). The deposition parameters for electro-spraying of MoS<sub>2</sub> over solar cell surface are tabulated in Table 1.

**2.4. Characterization Techniques.** The surface roughness and topography of the coated MoS<sub>2</sub> on the solar cells were examined through atomic force microscopy (AFM). X-ray diffraction (XRD) was used for analyzing the structural properties and crystallinity of calcinated MoS<sub>2</sub> sample. The layer thickness of the coated MoS<sub>2</sub> and surface morphology were interpreted from the results of field emission scanning electron microscopy (FE-SEM). The Raman analysis was performed to study the vibrational modes of the synthesized samples using Micro Raman spectroscopy from LabRAM HR Evolution, HORIBA France. The current-voltage relationships and resistivity of all the samples were determined through I-V analysis and the four-probe method, respectively. The transmittance and reflectance of the MoS<sub>2</sub>-coated samples and uncoated samples were inspected through optical analysis. The infrared thermal imaging technique was used to capture thermal images, and the temperature changes on the cells due to the coating were studied.

### 3. Result and Discussion

The XRD result of calcinated transition metal dichalcogenide MoS<sub>2</sub> at 900°C was compared with the standard MoS<sub>2</sub> diffraction data (JCPDS card No. 00-037-1492). The comparison of diffraction peaks with the standard file confirmed its cubic crystal arrangement as the diffraction peaks match precisely. The sharp diffraction peaks indicate the high crystalline nature of the synthesized MoS<sub>2</sub> powder. The interpreted miller indices of the ARC material were (100),

(101), (102), (103), (106), (105), (106), (110), (008), and (108). Figure 2 depicts the observed diffraction peaks of sol-gel synthesized MoS<sub>2</sub>.

The crystallite size was calculated using the basic equation of the Scherrer formula:

$$t = \frac{k \lambda}{\beta \cos \theta}. \quad (1)$$

Microstrain is defined as the RMS value of variation in lattice parameters across individual crystallites. It is also known as the ratio of peak width to peak position of obtained diffraction peaks. Dislocation density was the measure of number of dislocations within the unit volume of a crystalline material, i.e., number of lines of dislocation per unit volume. The dislocation density and microstrain of coating materials were determined using following equations and in Table 2.

$$\delta = \frac{1}{t^2}, \quad (2)$$

$$\epsilon = \frac{\beta}{4 \times \tan \theta},$$

where  $t$  is the average size of crystallite (nm),  $k$  is the Scherrer constant,  $\lambda$  is the X-ray wavelength (Å),  $\delta$  is the dislocation density (nm<sup>-2</sup>),  $\epsilon$  is the microstrain (radians),  $\beta$  is the line broadening at FWHM (radians), and  $\theta$  is the Bragg's angle (degree).

Further, a confirmative analysis was performed using the facile Raman spectroscopic measurement to analyze the vibrational modes obtained via sol-gel synthesized MoS<sub>2</sub> as shown in Figure 3. The sample revealed two bands at approximately 350 cm<sup>-1</sup> and 408 cm<sup>-1</sup> which are related to the  $E_{2g}^1$  (in-plane optical vibration of the Mo-S bond) and  $A_{1g}$  (out-of-plane optical vibrational mode of S atom),

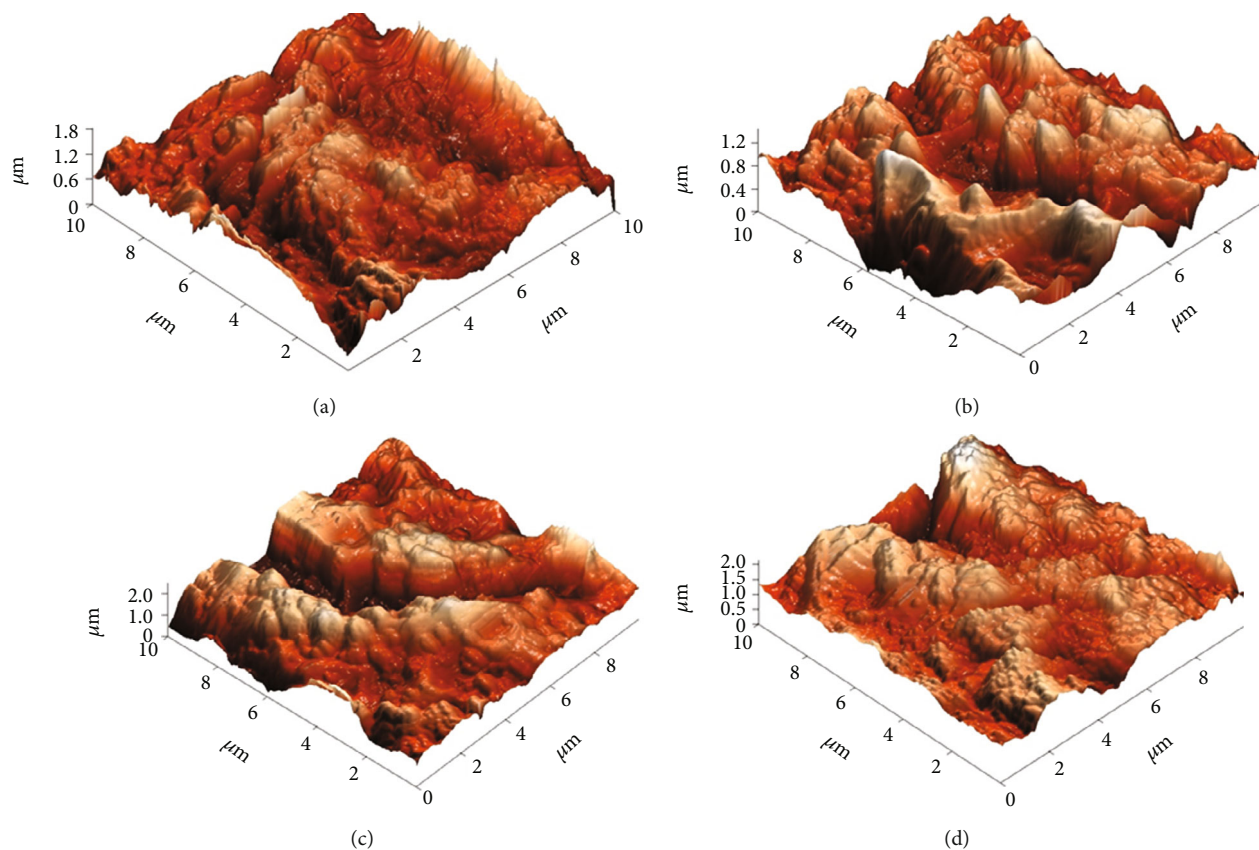


FIGURE 4: AFM results showing the topography of samples in 3D: (a) A-II, (b) A-III, (c) A-IV and (d) A-V.

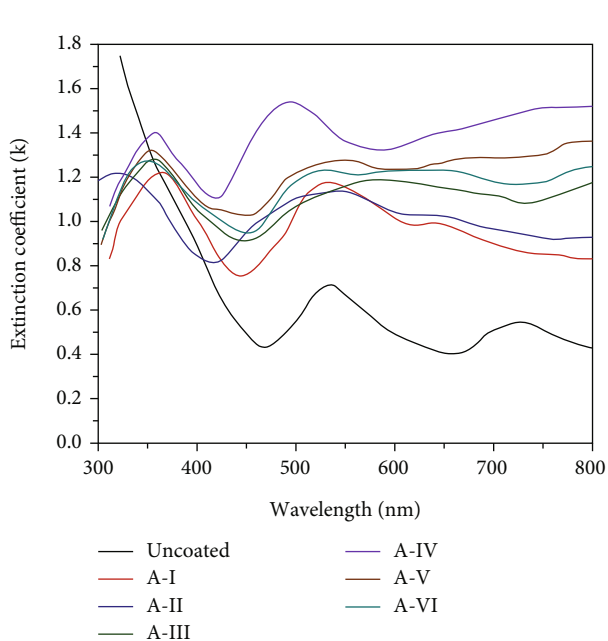


FIGURE 5: Extinction coefficient of various MoS<sub>2</sub>-coated solar cells.

respectively, thereby confirming the formation of MoS<sub>2</sub> which is well supported by XRD. These two vibrational modes occurred due to the vibrations in S-Mo-S layers.

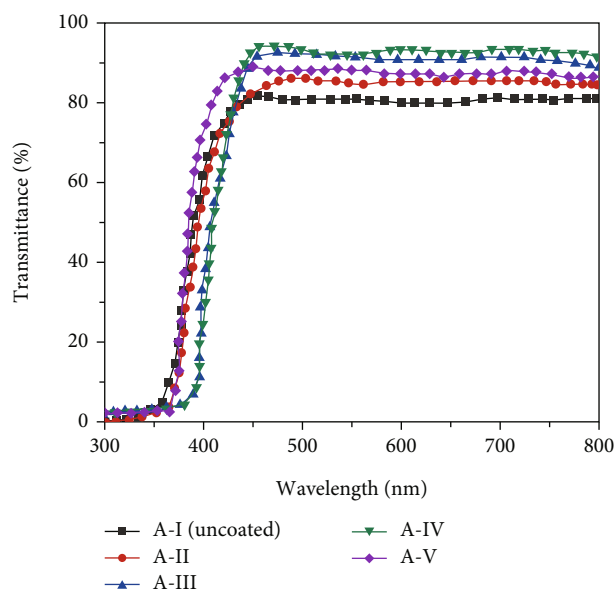


FIGURE 6: Transmittance of bare cell and MoS<sub>2</sub>-coated cells.

Through AFM analysis, surface topography of coated samples was analyzed. The surface roughness of the coating was a viable parameter in the aspect of reflective losses, as rough surface results in higher transmittance values. The AFM result was used to find out the root mean square



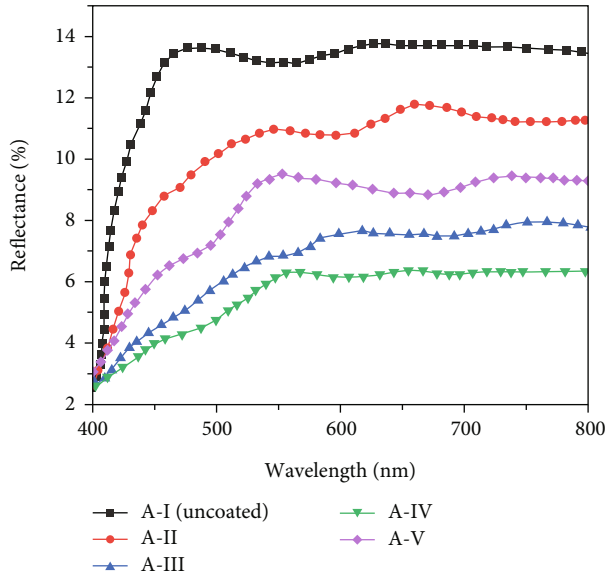
FIGURE 7: Reflectance of bare cell and MoS<sub>2</sub>-coated cells.

TABLE 3: Observed transmittance and reflectance percentage of bare and coated solar cells.

Sample	Coating thickness (nm)	Surface roughness (nm)	Transmittance (%)	Reflectance (%)
A-I	—	46	83.7	13.6
A-II	320	79	86.4	11.69
A-III	567	97	91.2	7.46
A-IV	746	124	93.6	6.3
A-V	938	153	89.3	9.75

TABLE 4: I-V measurement values for the samples under direct sunlight.

Samples	Open circuit voltage (V)	Short circuit current density (mA/cm <sup>2</sup> )	Fill factor (%)	Power conversion efficiency (%)
A-I	0.627	31.2	0.74	14.48
A-II	0.629	32.5	0.753	15.44
A-III	0.632	33.89	0.758	16.24
A-IV	0.651	36.3	0.76	17.96
A-V	0.636	34.06	0.754	16.33
A-VI	0.643	35.01	0.76	17.11

(RMS) roughness value of the coated samples. The roughness value of the samples increases with respect to coating time [40]. The obtained surface roughness of A-I–A-VI samples were 46 nm, 79 nm, 97 nm, 124 nm, 153 nm, and 176 nm. The surface topography of the coated samples A-II to A-V in three-dimensional view is shown in Figure 4. From experimentation, it was evident that increased coating time increases the surface roughness and coating thickness of deposited thin film. The calculated error values of measured surface roughness of samples A-I to A-VI were

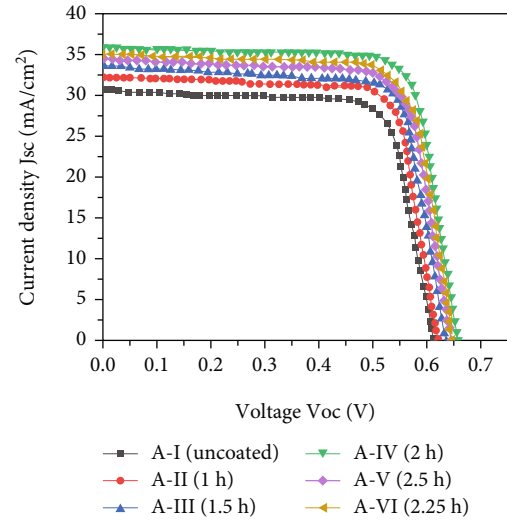


FIGURE 8: I-V plot of the samples under direct sunlight.

TABLE 5: Values of I-V measurement of samples under a controlled environment.

Samples	Open circuit voltage (V)	Short circuit current density (mA/cm <sup>2</sup> )	Fill factor (%)	Power conversion efficiency (%)
A-I	0.631	32.9	0.74	15.36
A-II	0.634	33.6	0.76	16.19
A-III	0.639	35.1	0.78	17.49
A-IV	0.647	37.3	0.78	18.82
A-V	0.641	36.2	0.77	17.87
A-VI	0.644	36.8	0.77	18.25

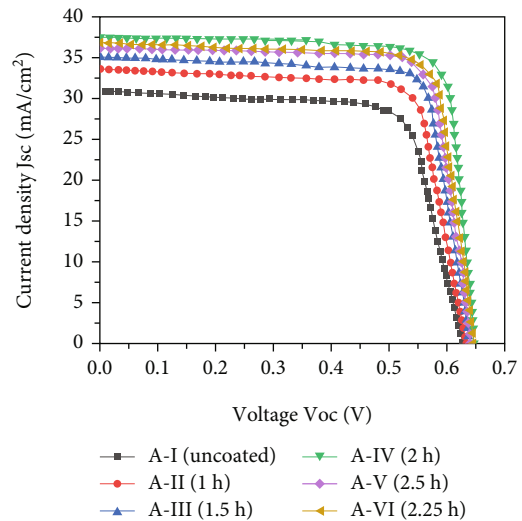


FIGURE 9: I-V plot of the samples under controlled source environment.

$\pm 1.47$ ,  $\pm 2.27$ ,  $\pm 1.41$ ,  $\pm 1.09$ ,  $\pm 3.03$ , and  $\pm 2.26$ . Up to optimal coating thickness, the light transmittance increases which allows more photons to get into the depletion region

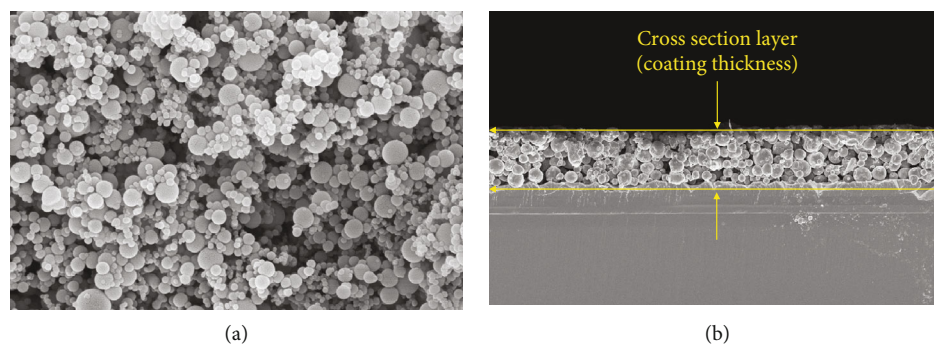


FIGURE 10: (a) Surface morphology of the A-IV-coated solar cell. (b) Cross-sectional view of the A-IV-coated solar cell.

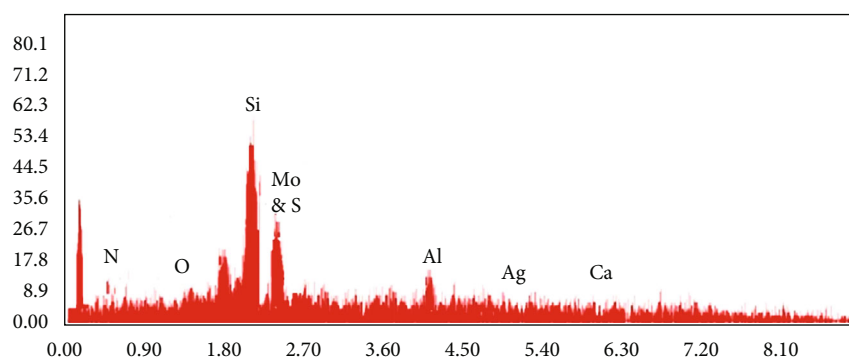


FIGURE 11: EDX analysis of A-IV-coated solar cell.

resulting in generation of more electrons in response with the incident photons.

Extinction coefficient was used to represent the magnitude of total amount of photons attenuated whenever the electromagnetic waves travel into the target material, as indicated in Figure 5. The higher absorption spectra were determined for the A-IV sample. The extinction coefficient was found to be maximum for the A-IV sample, resulting in lesser scattering of light than other coated and uncoated samples. From the observed results, the various  $\text{MoS}_2$ -coated solar cells facilitate more photons to enter into the depletion region than uncoated solar cells [41].

Within the UV visible spectra of wavelength 300 nm to 800 nm, the coating was highly transparent with the highest transmittance of 93.6% and lowest reflectance of 6.3%. Figures 6 and 7 illustrate the highest transmittance and minimum reflectance of the sample A-IV due to its high light trapping capacity. The increase in thickness of the coating layer until achieving optimal thickness results in high transmittance and low reflection for samples A-I to A-IV. Despite the increasing coating layer thickness for the sample A-V, a drop in transmittance and an increase in the reflection due to constructive interference were attained by coated particle agglomeration. Apart from the coating thickness, surface roughness also contributes for increasing the PCE of the solar cells. The samples with greater thickness than the optimal thickness offers a resistance to the light to pass into the depletion region resulting in decrement in efficiency of solar cell. Hence, the experiment was repeated for the time inter-

val of 2.15 hrs (A-V) and 2.30 hrs (A-VI) resulting in declined power output because the lesser number of photons was facilitating the power conversion process.

The relationship between the optical properties of the sample and its structural properties is consolidated in Table 3. The enhancement of electrical properties of the solar cells through antireflection coating was evaluated through performance analysis of coated and uncoated samples under a controlled and uncontrolled/open-source environment.

The generated power output for various  $\text{MoS}_2$ -coated and uncoated solar cells under direct sunlight is tabulated in Table 4. In an uncontrolled environment, the solar cells were analyzed under maximum solar radiation measured using solar radiation monitoring system (at 12.30 p.m.), for achieving maximum power conversion efficiency. From the results, it was found that power conversion efficiency increases with the increase in short circuit photocurrent density and open circuit voltage for coated solar cells. Sample A-IV exhibited maximum PCE of 17.96% ( $\text{VOC} = 0.651 \text{ V}$ ,  $\text{JSC} = 36.3 \text{ mA/cm}^2$ , and  $\text{FF} = 0.76$ ). Due to the increase in exciton generation, the I-V graph shifts gradually away from the origin. The fill factor is the maximum area of a quadrilateral plane accommodated under the I-V curve. Shifting of I-V curve away from the origin also increases the area under the curve leading to increase in fill factor. Photons of energy greater than the energy band gap of semiconducting material have the tendency to break the depletion region and expel as charge carrier. These

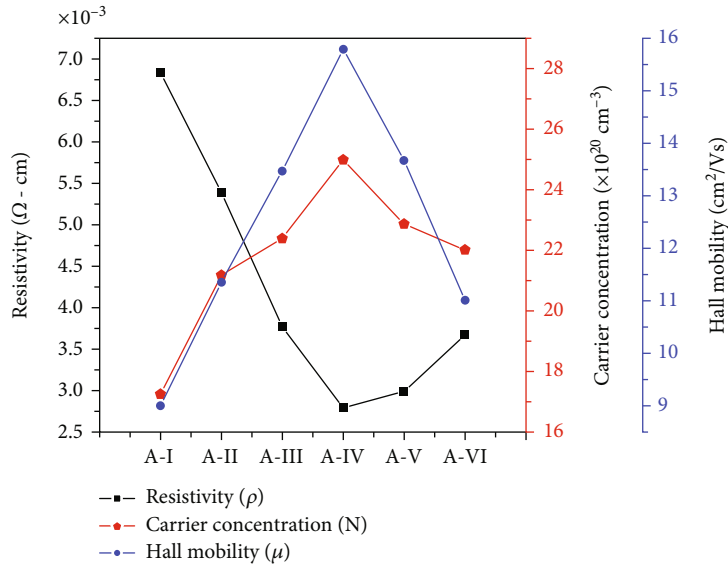


FIGURE 12: Resistivity analysis of various samples.

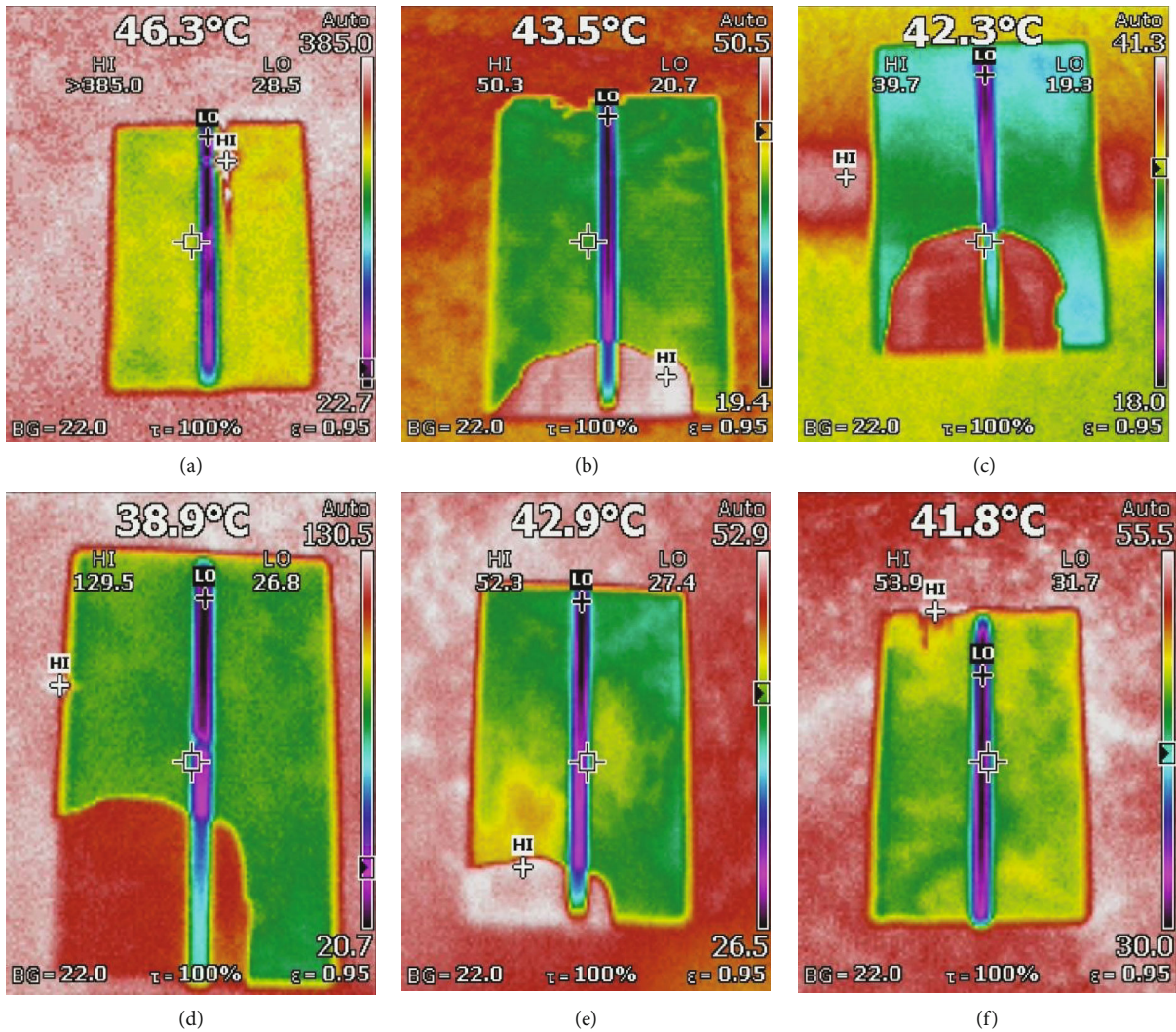


FIGURE 13: Temperature analysis under direct sunlight: (a) A-I (uncoated solar cell), (b) A-II, (c) A-III, (d) A-IV, (e) A-V, and (f) A-VI.



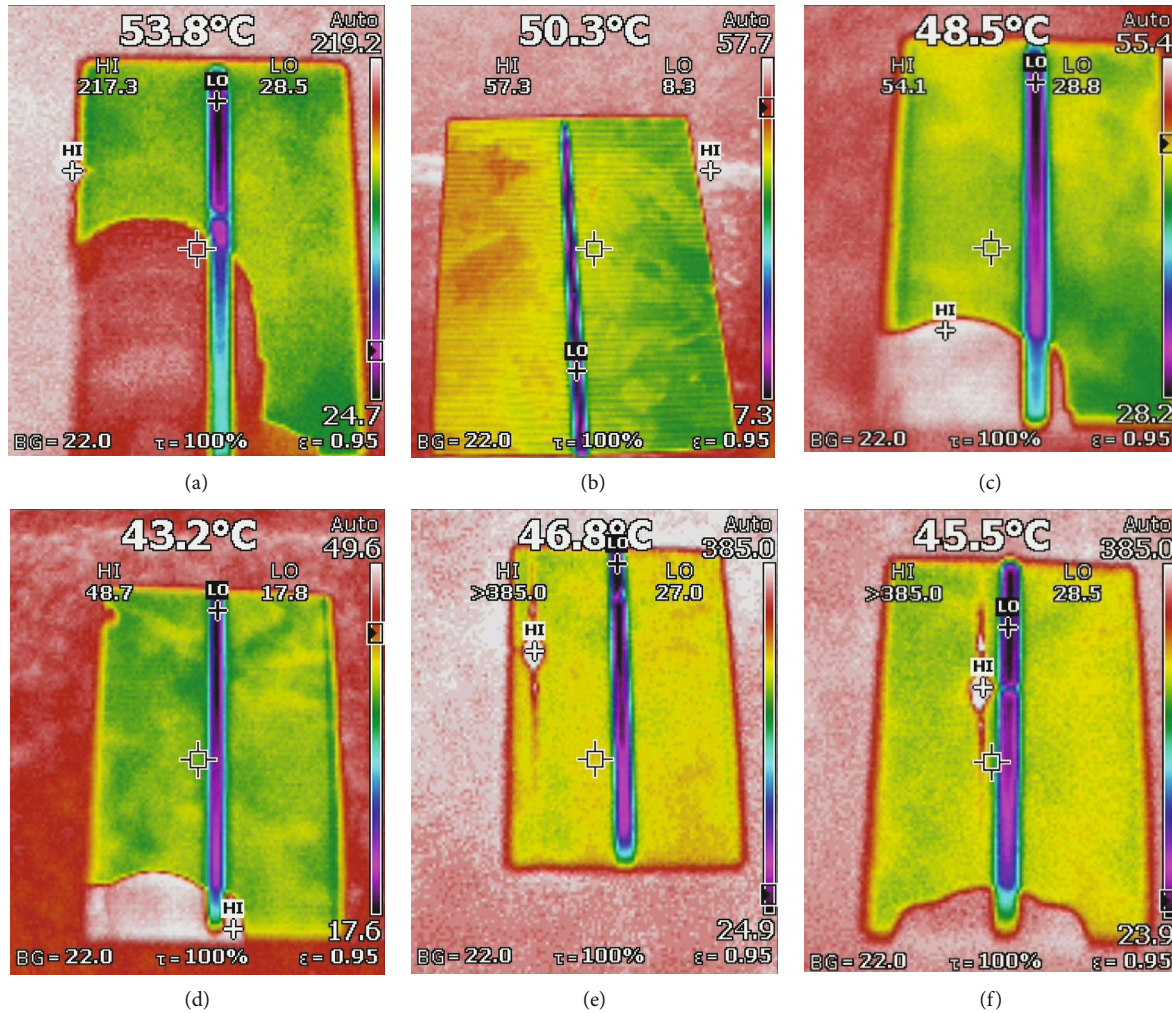


FIGURE 14: Temperature analysis under controlled source environment: (a) A-I (uncoated solar cell), (b) A-II, (c) A-III, (d) A-IV, (e) A-V, and (f) A-VI.

charge carriers were responsible for the power generation process in solar cells. All these analyses were performed with the aid of kick start interfacing software and Keithley 2450 I-V source meter along with a pyranometer. The decrease in transmittance of sample A-V led to a decline in electric output, which was clearly indicated in Figure 8.

The same steps were followed for both uncoated and  $\text{MoS}_2$  solar cells in the controlled environment, and the values are tabulated in Table 5. In a controlled source environment, an artificial solar setup regulated by alternating current was fabricated. To provide a steady source of radiation, neodymium lamp was used as the source of light with the radiation intensity prefixed as  $1000 \text{ W/m}^2$ . The output radiation of fabricated artificial solar setup was prefixed as  $1000 \text{ W/m}^2$ . The sample A-IV had shown prominent PCE of 18.82% compared to 15.36% PCE ( $\text{VOC} = 0.631 \text{ V}$ ,  $\text{JSC} = 32.9 \text{ mA/cm}^2$ , and  $\text{FF} = 0.74$ ) of the bare cell. Due to excessive heat flux incurred by light scattering, a decline in the efficiency of sample A-V was observed (as in Figure 9). The antireflective  $\text{MoS}_2$ -coated solar cells exert increasing efficiency until the coating thickness reaches optimal coating thickness. Further coating of  $\text{MoS}_2$

leads to poor transmittance of incident photons leading to the decreased power generation. This is also due to more scattering of incident light.

The cross-sectional thickness and surface morphology of the thin film coatings were studied using FESEM. The morphology of the layers and coating thickness depends on various coating constraints such as coating time, flow rate, distance of nozzle from the substrate, supply voltage, type of substrate, and substrate temperature [42]. Figure 10 displays the FESEM image of coating structure and its cross-sectional thickness. The cross-sectional thickness of the coated  $\text{MoS}_2$  was observed to be 320 nm, 567 nm, 746 nm, 938 nm, and 986 nm, especially for samples A-II to A-VI, respectively. From the obtained results, it was evident that the increase in coating time increases the coating thickness. The optimal coating thickness for achieving maximum performance was 746 nm (sample A-IV). This leads to phenomenal electrical properties and high PCE in the I-V analysis in both controlled and uncontrolled environments. The calculated error values of measured coating thickness of samples A-II to A-VI were  $\pm 1.31$ ,  $\pm 1.09$ ,  $\pm 2.08$ ,  $\pm 2.58$ , and  $\pm 2.20$ .

In addition to this, EDX analysis of best operating solar cell is indicated in Figure 11. EDX analysis shows the elements present in the inspected sample at various proportions.

The resistivity of the samples was obtained through four-probe method. The coated cells exhibited less resistivity than the bare uncoated cell. It can be associated with the existence of the Mo and S elements present in the surface of solar cell. The decline in the values of resistivity can be correlated with increase of conductivity resulting in high photocurrent density generation. The sample A-IV holds superior electrical properties with resistivity of  $2.79 \times 10^{-3} \Omega - \text{cm}$ . As compared to the resistance value of uncoated solar cell ( $6.83 \times 10^{-3} \Omega - \text{cm}$ ), sample A-IV had significantly lower resistivity values. The measure of movement of holes or electrons within the semiconductor or conductor material was termed as hall mobility [43]. The variations in the carrier concentration, hall mobility, and resistivity are cordially illustrated in Figure 12 [44, 45]. Coating of antireflective materials with increased grain size and reduced grain boundary results in increased exciton separation and recombination [9]. It was also found that resistivity drops with the increase in light transmittance for the electrosprayed  $\text{MoS}_2$ -coated solar cells. The A-IV sample possesses the ability to generate more photons because more number of excitons lie within the localized state of valence band [9, 46].

The temperature analysis of uncoated and  $\text{MoS}_2$ -coated solar cells was executed using IR thermal imaging technique under both controlled and uncontrolled environment as indicated in Figures 13 and 14. This method was employed widely in fields like welding, medicine, and manufacturing industries. The temperature of the solar cell affects the electrical performance of solar cell. Likewise, the efficiency of the solar cell seemed to decrease with the increase in the temperature for both controlled and uncontrolled environments [45, 47–49].

The sample A-IV possessed lower surface temperature than other solar cells in both controlled and uncontrolled environments. The observed reduction in transmittance of sample A-V and A-VI was due to the increased light scattering which leads to the increase in heat flux. The increase in scattering of electron-phonon leads to a decrease in PCE of the solar cells. Due to the reduction in mobility and charge carrier concentration, there is a declined PCE of solar cell [34, 35]. Hence,  $\text{MoS}_2$  acts as an excellent antireflective material for augmenting the PCE of the solar cell.

#### 4. Conclusion

$\text{MoS}_2$  was synthesized using the sol-gel method and employed as an antireflection coating for a polycrystalline silicon solar cell using electrospraying method. The samples were coated with varying deposition time under constant voltage of 17 kV. From XRD analysis, (100), (101), (102), (103), (106), (105), (106), (110), (008), and (108) were the obtained miller index values of synthesized crystalline  $\text{MoS}_2$ . The obtained diffraction peaks precisely matched with the standard data of the  $\text{MoS}_2$  confirming the crystalline nature of synthesized material. The dislocation density and microstrain were calculated for the synthesized material

identified using the observed XRD results. The thickness of the coatings was observed as 320 nm, 567 nm, 746 nm, 938 nm, and 859 nm through the results of FESEM. With the aid of I-V and optical analysis, the influential factors such as photogenerated current and voltage, surface roughness, and thickness of the coating were identified. A-IV solar cell experiences highest PCE of 17.96% under direct sunlight and 18.82% in a controlled source environment. Comparatively, there was a phenomenal increase in the current density of 13% higher than the uncoated solar cell especially generated by 120 min coated solar cell. The resistivity values were reduced to minimum of  $2.79 \times 10^{-3} \Omega - \text{cm}$  than the other solar cells. The coated cells hold greater optical properties with highest transmittance and lowest reflectance of 93.6% and 6.3%, respectively. The sample A-IV facilitates more photons to pass through the coating reducing the scattering of light. Hence, synthesized  $\text{MoS}_2$  holds the antireflective property and can be employed for attaining maximum power conversion efficiency of polycrystalline Si solar cells.

#### Data Availability

All data generated or analyzed during this study are included in this published manuscript.

#### Additional Points

*Highlights.* (i) The power conversion efficiency of polycrystalline solar cell is augmented with ARC. (ii) An antireflection coating is made by molybdenum disulphide through sol-gel method. (iii) Electrospraying method is employed for fine distribution of ARC. (iv) The surface roughness and coating thickness were correlated to the increase in PCE of solar cells

#### Conflicts of Interest

The authors declare that they have no conflicts of interest.

#### Acknowledgments

Author V. K. Gobinath acknowledges the Department of Science & Technology (DST), Government of India, for the successful execution of this research work through the Teachers Associateship for Research Excellence (Ref No. TAR/2021/000173).

#### References

- [1] O. Ellabban, H. Abu-Rub, and F. Blaabjerg, "Renewable energy resources: current status, future prospects and their enabling technology," *Renewable and Sustainable Energy Reviews*, vol. 39, pp. 748–764, 2014.
- [2] A. R. Jordehi, "Parameter estimation of solar photovoltaic (PV) cells: a review," *Renewable and Sustainable Energy Reviews*, vol. 61, pp. 354–371, 2016.
- [3] C. Xu, Z. Zhao, K. Yang et al., "Recent progress in all-small-molecule organic photovoltaics," *Journal of Materials Chemistry A*, vol. 10, no. 12, pp. 6291–6329, 2022.

- [4] K. Yang, Z. Zhao, M. Liu et al., "Employing liquid crystal material as regulator to enhance performance of photomultiplication type polymer photodetectors," *Chemical Engineering Journal*, vol. 427, article 131802, 2022.
- [5] C. Xu, K. Jin, Z. Xiao et al., "Efficient semitransparent layer-by-layer organic photovoltaics via optimizing wide bandgap and narrow absorption polymer layer thickness," *Solar RRL*, vol. 6, no. 8, p. 2200308, 2022.
- [6] S. Mekhilef, R. Saidur, and M. Kamalisarvestani, "Effect of dust, humidity and air velocity on efficiency of photovoltaic cells," *Renewable and Sustainable Energy Reviews*, vol. 16, no. 5, pp. 2920–2925, 2012.
- [7] C. Agustín-Sáenz, J. Á. Sánchez-García, M. Machado, M. Brizuela, O. Zubillaga, and A. Tercjak, "Broadband antireflective coating stack based on mesoporous silica by acid-catalyzed sol-gel method for concentrated photovoltaic application," *Solar Energy Materials and Solar Cells*, vol. 186, pp. 154–164, 2018.
- [8] G. V. Kaliyannan, S. V. Palanisamy, M. Palanisamy, M. Subramanian, P. Paramasivam, and R. Rathanasamy, "Development of sol-gel derived gahnite anti-reflection coating for augmenting the power conversion efficiency of polycrystalline silicon solar cells," *Materials Science-Poland*, vol. 37, no. 3, pp. 465–472, 2019.
- [9] S. Sivaraj, R. Rathanasamy, G. Velu Kaliyannan, and M. Palanisamy, "Surface coatings of zinc oxide–tantalum pentoxide on multicrystalline Si solar cell as effective light harvester," *Journal of Materials Science: Materials in Electronics*, vol. 33, pp. 17699–17710, 2022.
- [10] S. Sivaraj, R. Rathanasamy, G. V. Kaliyannan et al., "A comprehensive review on current performance, challenges and progress in thin-film solar cells," *Energies*, vol. 15, no. 22, p. 8688, 2022.
- [11] R. Goyal, S. Lamba, and S. Annapoorni, "Growth of cobalt nanoparticles in  $\text{co-Al}_2\text{O}_3$  thin films deposited by RF sputtering," *Physica Status Solidi*, vol. 213, no. 5, pp. 1309–1316, 2016.
- [12] S.-Y. Lien, D.-S. Wu, W.-C. Yeh, and J.-C. Liu, "Tri-layer antireflection coatings ( $\text{SiO}_2/\text{SiO}_2\text{-TiO}_2/\text{TiO}_2$ ) for silicon solar cells using a sol-gel technique," *Solar Energy Materials and Solar Cells*, vol. 90, no. 16, pp. 2710–2719, 2006.
- [13] R. Rathanasamy, G. Velu Kaliyannan, S. Sivaraj et al., "Influence of silicon dioxide-titanium dioxide antireflective Electro-sprayed coatings on multicrystalline silicon cells," *Advances in Materials Science and Engineering*, vol. 2022, Article ID 9444524, 11 pages, 2022.
- [14] J.-H. Lee, K.-H. Ko, and B.-O. Park, "Electrical and optical properties of ZnO transparent conducting films by the sol-gel method," *Journal of Crystal Growth*, vol. 247, no. 1-2, pp. 119–125, 2003.
- [15] S. Goktas and A. Goktas, "A comparative study on recent progress in efficient ZnO based nanocomposite and heterojunction photocatalysts: a review," *Journal of Alloys and Compounds*, vol. 863, article 158734, 2021.
- [16] Q. M. Wang, T. F. Zhang, S. H. Kwon, and K. H. Kim, "Fabrication of  $\text{TiO}_2$  films on glass substrates by a pulsed dc reactive magnetron sputtering," *Applied Mechanics and Materials*, vol. 71-78, pp. 5050–5053, 2011.
- [17] W. Choi, N. Choudhary, G. H. Han, J. Park, D. Akinwande, and Y. H. Lee, "Recent development of two-dimensional transition metal dichalcogenides and their applications," *Materials Today*, vol. 20, no. 3, pp. 116–130, 2017.
- [18] D. Gupta, V. Chauhan, and R. Kumar, "A comprehensive review on synthesis and applications of molybdenum disulfide ( $\text{MoS}_2$ ) material: past and recent developments," *Inorganic Chemistry Communications*, vol. 121, article 108200, 2020.
- [19] M. Chinnasamy, R. Rathanasamy, S. Sivaraj et al., "Effective Utilization of Synthesized  $\text{FeS}_2$  for Improving Output Performance of Polycrystalline Silicon Solar Cell," *Advances in Materials Science and Engineering*, vol. 2022, Article ID 1252105, 10 pages, 2022.
- [20] A. S. Sarkun, N. Ekren, and Ş. Sağlam, "A review of anti-reflection and self-cleaning coatings on photovoltaic panels," *Solar Energy*, vol. 199, pp. 63–73, 2020.
- [21] L. Xu, X. Li, Y. Chen, and F. Xu, "Structural and optical properties of ZnO thin films prepared by sol-gel method with different thickness," *Applied Surface Science*, vol. 257, no. 9, pp. 4031–4037, 2011.
- [22] M. A. Baghchesara, R. Yousefi, M. Cheraghizade, F. Jamali-Sheini, and A. Saædi, "Photocurrent application of Zn-doped CdS nanostructures grown by thermal evaporation method," *Ceramics International*, vol. 42, no. 1, pp. 1891–1896, 2016.
- [23] S. Rozati and S. Akesteh, "Characterization of ZnO: Al thin films obtained by spray pyrolysis technique," *Materials Characterization*, vol. 58, no. 4, pp. 319–322, 2007.
- [24] M. Dohi, "Thin film formation of  $\text{EuGa}_2\text{S}_4$  by rf sputtering and improvement of film transmittance," *Physica Status Solidi C*, vol. 10, no. 7-8, pp. 1115–1118, 2013.
- [25] G. V. Kaliyannan, R. Rathanasamy, S. Sivaraj, M. Chinnasamy, and S. Kandasamy, "An Extensive Review Owing to the Influence of Surface Coating on the Technical Performance of Solar Cells," in *Advances in Functional and Smart Materials. Lecture Notes in Mechanical Engineering*, C. Prakash, S. Singh, and G. Krolczyk, Eds., Springer, Singapore, 2023.
- [26] P. S. T. Sai, K. Sharma, K. Devarayapalli, and J. R. Rao, "GO- $\text{TiO}_2$  nano composites for silicon PV cell application," *Materials Today: Proceedings*, vol. 2, no. 9, pp. 4557–4562, 2015.
- [27] Y. S. Kim and S. J. Yun, "Studies on polycrystalline ZnS thin films grown by atomic layer deposition for electroluminescent applications," *Applied Surface Science*, vol. 229, no. 1-4, pp. 105–111, 2004.
- [28] J. Patel, F. Mighri, A. Ajji, D. Tiwari, and T. K. Chaudhuri, "Spin-coating deposition of PbS and CdS thin films for solar cell application," *Applied Physics A*, vol. 117, no. 4, pp. 1791–1799, 2014.
- [29] G. V. Kaliyannan, S. V. Palanisamy, E. Priyanka, S. Thangavel, S. Sivaraj, and R. Rathanasamy, "Investigation on sol-gel based coatings application in energy sector - A review," *Materials Today: Proceedings*, vol. 45, pp. 1138–1143, 2021.
- [30] X. Guo, Z. Wang, W. Zhu, and H. Yang, "The novel and facile preparation of multilayer  $\text{MoS}_2$  crystals by a chelation-assisted sol-gel method and their electrochemical performance," *RSC Advances*, vol. 7, no. 15, pp. 9009–9014, 2017.
- [31] A. Jaworek and A. T. Sobczyk, "Electrospraying route to nanotechnology: an overview," *Journal of Electrostatics*, vol. 66, no. 3-4, pp. 197–219, 2008.
- [32] O. V. Salata, "Tools of nanotechnology: electrospray," *Current Nanoscience*, vol. 1, no. 1, pp. 25–33, 2005.
- [33] S. Prashanth, R. Rajasekar, V. Gobinath, G. Raja, K. Subha, and K. Manjunath, "Augmenting the performance of photovoltaic cell through surface coating of molybdenum disulfide," *Chalcogenide Letters*, vol. 18, pp. 161–170, 2021.



- [34] B. Kivrak and M. Akyol, "Investigation of the effect of solvent and heat treatment process on structural properties of MoS<sub>2</sub> thin films," *Dokuz Eylul University*, vol. 24, pp. 81–90, 2022.
- [35] M. Khan, S. Ali, N. Alwadai et al., "Structural, electrical and optical properties of hetrostructured MoS<sub>2</sub>/ZnO thin films for potential perovskite solar cells application," *Journal of Materials Research and Technology*, vol. 20, pp. 1616–1623, 2022.
- [36] M. V. Nardi, M. Timpel, G. Ligorio et al., "Versatile and scalable strategy to grow sol-gel derived 2H-MoS<sub>2</sub> thin films with superior electronic properties: a memristive case," *ACS Applied Materials & Interfaces*, vol. 10, no. 40, pp. 34392–34400, 2018.
- [37] R. Singh and S. Tripathi, "Structural and optical properties of few-layer MoS<sub>2</sub> thin films grown on various substrates using RF sputtering process," *Journal of Materials Science: Materials in Electronics*, vol. 30, no. 8, pp. 7665–7680, 2019.
- [38] P. Shanmugam, R. Rathanasamy, G. V. Kaliyannan, S. Sivaraj, M. Chinnasamy, and M. S. Anbupalani, "Performance enhancement of polycrystalline silicon solar cell through sputter coated molybdenum disulphide surface films," *Materials Science*, vol. 28, no. 2, pp. 157–163, 2022.
- [39] A. Pugalenti, R. Balasundaraprabhu, S. Prasanna, K. Thilagavathy, N. Muthukumarasamy, and S. Jayakumar, "Effect of substrate temperature on structural, morphology and optical properties of RF magnetron sputtered CZT thin films," *Materials Technology*, vol. 30, no. 4, pp. 200–204, 2015.
- [40] Q. Hou, F. Meng, and J. Sun, "Electrical and optical properties of Al-doped ZnO and ZnAl<sub>2</sub>O<sub>4</sub> films prepared by atomic layer deposition," *Nanoscale Research Letters*, vol. 8, no. 1, pp. 1–8, 2013.
- [41] R. Singh and S. Tripathi, "Evaluation of optical parameters and characterization of few layer sputtered MoS<sub>2</sub> film by spectroscopic ellipsometry," *Optical and Quantum Electronics*, vol. 51, no. 10, pp. 1–16, 2019.
- [42] A. Taherniya and D. Raoufi, "Thickness dependence of structural, optical and morphological properties of sol-gel derived TiO<sub>2</sub> thin film," *Materials Research Express*, vol. 6, article 016417, 2019.
- [43] A. Tumbul, A. Göktaş, M. Z. Zarbali, and F. Aslan, "Structural, morphological and optical properties of the vacuum-free processed CZTS thin film absorbers," *Materials Research Express*, vol. 5, no. 6, article 066408, 2018.
- [44] C. Lee, W. Yang, and R. G. Parr, "Development of the Colle-Salvetti correlation-energy formula into a functional of the electron density," *Physical Review B*, vol. 37, no. 2, pp. 785–789, 1988.
- [45] H. Kawazoe and K. Ueda, "Transparent conducting oxides based on the spinel structure," *Journal of the American Ceramic Society*, vol. 82, no. 12, pp. 3330–3336, 1999.
- [46] G. Velu Kaliyannan, S. V. Palanisamy, R. Rathanasamy et al., "An extended approach on power conversion efficiency enhancement through deposition of ZnS-Al<sub>2</sub>S<sub>3</sub> blends on silicon solar cells," *Journal of Electronic Materials*, vol. 49, no. 10, pp. 5937–5946, 2020.
- [47] S. Dubey, J. N. Sarvaiya, and B. Seshadri, "Temperature dependent photovoltaic (PV) efficiency and its effect on PV production in the world - a review," *Energy Procedia*, vol. 33, pp. 311–321, 2013.
- [48] I. B. Karki, "Effect of temperature on the I-V characteristics of a polycrystalline solar cell," *Journal of Nepal Physical Society*, vol. 3, no. 1, pp. 35–40, 2016.
- [49] J. Kumar, V. S. Negi, K. D. Chattopadhyay, R. V. Sarepaka, and R. K. Sinha, "Thermal effects in single point diamond turning: analysis, modeling and experimental study," *Measurement*, vol. 102, pp. 96–105, 2017.